We are IntechOpen, the world's leading publisher of Open Access books Built by scientists, for scientists

4,800
Open access books available

122,000
International authors and editors

135M
Downloads

Our authors are among the

154
Countries delivered to

TOP 1%
most cited scientists

12.2%
Contributors from top 500 universities

CLARIVATE ANALYTICS BOOK CITATION INDEX INDEXED

WEB OF SCIENCE™

Selection of our books indexed in the Book Citation Index in Web of Science™ Core Collection (BKCI)

Interested in publishing with us?
Contact book.department@intechopen.com

Numbers displayed above are based on latest data collected.
For more information visit www.intechopen.com

23

On the Behavior of FRP-to-concrete Adhesive Interface: Theoretical Models and Experimental Results

Enzo Martinelli, Antonio Bilotta, Ciro Faella and Emidio Nigro
Department of Civil Engineering, University of Salerno, Fisciano (SA),
Department of Structural Engineering, University of Naples "Federico II", Naples
Italy

1. Introduction

Fiber-reinforced polymers (FRP) are more and more commonly employed for strengthening existing structures of both reinforced concrete (RC) and masonry. Since FRP sheets (cured in situ) or plates (preformed) are externally bonded on a concrete or masonry substrate, the issue of adhesion on those materials generally controls the effectiveness of strengthening in members stressed either in bending or shear (Motavalli & Czaderski, 2007).

The use of composite materials for structural strengthening of civil structures and infrastructures began with some pioneering application at the middle of the '80s (Meier, 1987) of the past century.

Plenty of experimental work and theoretical investigations have been carried out in the following years with the aim of demonstrating the feasibility of strengthening civil structures by means of composite materials (Swamy et al., 1987; Meier, 1995). However, composite materials were already widely used in other fields of structural engineering, such as aerospace (Hart-Smith, 1973), aeronautics and, later, automotive. Thus, the initial research activities about the possible use of composites in civil structures were not mainly focused on the behavior of composites themselves. They were rather intended at addressing two main issues regarding, on the one hand, the different behavior of composites with respect to more traditional materials (basically, steel) commonly used as a reinforcement in civil structures (Arduini & Nanni, 1997; Naaman et al., 2001; Triantafillou et al., 2001) and, on the other hand, the aspects related to the adhesive connection of the FRP laminates to the concrete (or masonry) substrate (Täljsten, 1997; Neubauer & Rostasy, 1997).

The main findings of the research activities carried out in the '90s contributed to guidelines (fib, 2001; CNR-DT200, 2004; ACI 440-2R-08) for designing FRP-based strengthening intervention of RC and masonry members.

Bonding between FRP laminates (sheets or plates) and concrete emerged as a cutting-edge issue from the first decade of research activities on composite materials for civil structures. In particular, several failure modes due to loss of adhesion between the externally bonded FRP element and the concrete substrate have been observed experimentally and recognized as specific features of this kind of members (Meier, 1995; Bonacci, 1996).

As a matter of principle, the following seven failure modes have been defined in the scientific literature (Teng et al., 2002):

a. flexural failure by FRP rupture;
b. flexural failure by crushing of compressive concrete;
c. shear failure;
d. concrete cover separation;
e. plate end interfacial debonding;
f. intermediate flexural crack induced interfacial debonding;
g. intermediate flexural-shear crack induced interfacial debonding.

The last three failure modes are actually related to debonding failure of the FRP laminate from the concrete substrate. Local failure possibly induced by irregularities in the substrate surface can be also observed. Fig. 1 represents those failure modes pointing their typical position throughout the FRP-to-composite adhesive interface.

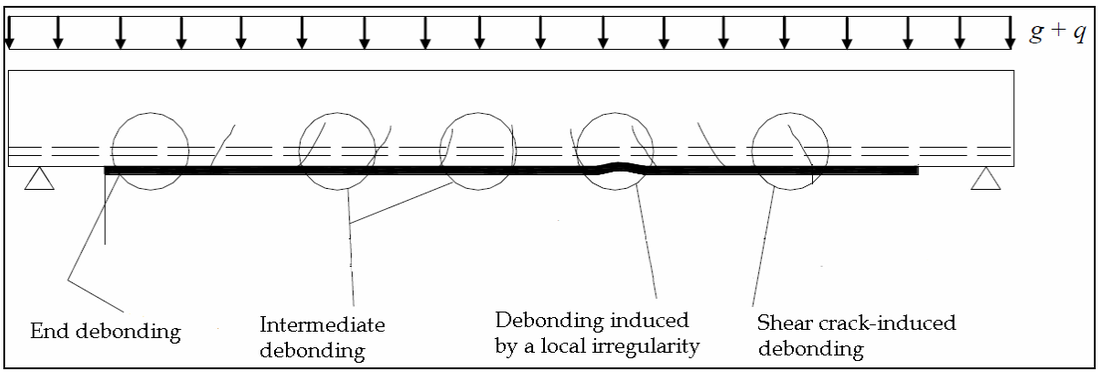

Fig. 1. Possible failure modes due to debonding in RC beams externally strengthened by FRP

Analytical studies have been carried out for determining the actual distribution of stresses throughout the adhesive interface. In particular, well-established elastic models, already used within the framework of structural mechanics, have been proposed as simplified practical methods for determining both shear and normal (peeling) stresses at the FRP-to-concrete interface (Roberts, 1989; Malek et al., 1998; Rabinovich & Frostig, 2000). However, those simplified methods were generally based on the assumption of an elastic behaviour of the above mentioned interface. Although this assumption can be considered under service loads, it cannot be generally accepted for the load values close to the onset of debonding. Micro-cracking phenomena develop as the levels of the interface stresses cannot be resisted by concrete, resulting in a highly nonlinear behaviour for the FRP-to-concrete interface which can be modelled by means of several possible relationships between interface stresses and displacements (Lu et al, 2005). Consequently, more advanced numerical models have been also proposed for simulating the actual distribution of stresses looking after the various fracture phenomena developing in concrete beneath the adhesive interface (Rabinovich & Frostig, 2000; Faella et al., 2008).

More recently, several models have been proposed in the scientific literature for predicting the strength of beams against both plate end-debonding and intermediate-debonding (Smith & Teng, 2001; Teng et al., 2003). They generally derive by mechanical observations carried out on the behaviour of FRP laminates glued on concrete blocks (Täljsten, 1996) and tested in pullout with the aim of measuring some relevant quantities, such as the ultimate strength

at debonding and the axial strain distribution throughout the FRP bonded length (Chajes et al., 1996).

Understanding the behaviour of FRP-to-concrete joints tested under pull-out actions is of paramount importance for describing the key mechanical properties of the adhesive interface between FRP and concrete, which plays a key role in the possible debonding failure of externally strengthened beams. Thus, advanced testing and monitoring techniques have been also used for a deeper investigation of the behaviour of those joints (Czaderski et al., 2010). The experimental results obtained by the mentioned pull-out tests can be considered for identifying the non-linear relationships connecting interface stresses and displacements (Faella et al., 2009). In particular, a bilinear elastic-softening relationship between the interface shear stress and the corresponding displacements is often used for the FRP-to-concrete interface. The elastic branch of that stress-strain relationship results from the elastic behaviour of both the adhesive layer and the concrete substrate, mainly stressed in shear. The slope of such an elastic branch (namely, the "slip modulus" according to Lee et al, 1999) is generally much smaller than the value corresponding to the ration between the shear modulus of the resin and its thickness, as it would be determined by assuming a fully stiff behaviour of the concrete block (Faella et al., 2002).

A closed-form analytical solution has been derived in Faella et al. (2002) for the distribution of both shear stresses and relative slips in FRP-to-concrete joints with a bilinear adhesive interface. Further advances have been proposed by Lu et al. (2005), while the influence of different assumptions on the shape of the stress-slip relationship (i.e. bilinear, linearly softening, rigid-plastic, and so on) is discussed in both Chen & Teng (2001) and Wu et al. (2002). However, the fracture energy G_F (Täljsten, 1996) is the key parameter characterizing any various shear-stress-interface-slip relationship. The ultimate pull-out strength of the FRP-to-concrete joints is controlled by that parameter as well as the axial stiffness of the laminate and the bonding length. A limit value of the bonding length beyond which no further increases of the ultimate pull-out force can be observed; it is generally referred as "transfer length" (Bizindavyi & Neale, 1999). Some concepts of Fracture Mechanics are more and more employed in modelling the overall behaviour of both FRP laminates connected to concrete blocks (Yuan et al., 2007) and RC beams externally strengthened by FRP (Rabinovitch & Frostig, 2001; Achintha & Burgoygne, 2008).

The present chapter deals with the mechanical behaviour of the adhesive interface between FRP and concrete, proposing a wide overview of some theoretical models and experimental results which can be useful for understanding such a behaviour.

In the second section, an analytical model will be firstly presented for determining both shear and normal stresses throughout the adhesive interface in the linear range. The nonlinear behaviour of the FRP-to-concrete interface will be also addressed by discussing the ultimate bearing capacity of FRP laminates bonded on concrete members.

The third section will present the features of the most well-established testing techniques for investigating the mechanical behaviour of FRP-to-concrete interface, from the early loading stages up to failure. A series of experimental results of pull-out tests on FRP laminates will be also presented for pointing out the most important behavioural characteristics of the FRP-to-concrete interface in the case of both sheets and plates.

Finally, the fourth section will present some of the most recent design formulae which can be derived by the above mentioned theoretical models and calibrated on the available experimental results, partly reported in the present chapter.

2. Theoretical models

An analytical formulation for modelling the behaviour of the FRP-to-concrete adhesive interfaces is presented and discussed in the present section. The behaviour of FRP-to-concrete joints in the linear range is examined in the first subsection. Then, the aspects more directly related at the ultimate behaviour are addressed in the second one.

2.1 A general analytical model: formulation in the linear range

A simplified model is formulated in the present section with the aim of simulating the behaviour of FRP laminates bonded on concrete and tested in pull-out, simulating how both the in-plane (namely, "slip") and out-of-plane displacement components develop throughout the FRP length. It is based on the following assumptions:

- the FRP strip is simulated as a Bernoulli beam;
- the adhesive layer is modelled as a bi-dimensional elastic domain in plane deformations.

The generalized forces N, V, M applied on the transverse section of the strip at the abscissa z and the interface stresses (shear τ and normal σ, respectively) are represented in Fig. 2. The following equilibrium equations can be stated between those force and stress components:

$$\frac{dN}{dz} + \tau_f b_f = 0 \ , \tag{1}$$

$$\frac{dV}{dz} = -b_f \sigma_y \ , \tag{2}$$

$$\frac{dM}{dz} + \tau_f \frac{b_f t_f}{2} - V = 0 \ . \tag{3}$$

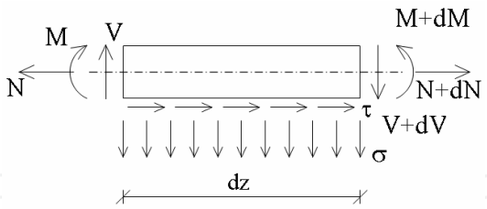

Fig. 2. Forces on the segmental FRP strip element

The parameters v, w and φ completely describe the displacement field of the strip and the following compatibility equations relate them to the axial strain ε and the curvature χ (Fig. 3):

$$\varepsilon = \frac{dw}{dz} \ , \tag{4}$$

$$\chi = \frac{d\varphi}{dz} \ , \tag{5}$$

$$\varphi = -\frac{dv}{dz} \ . \tag{6}$$

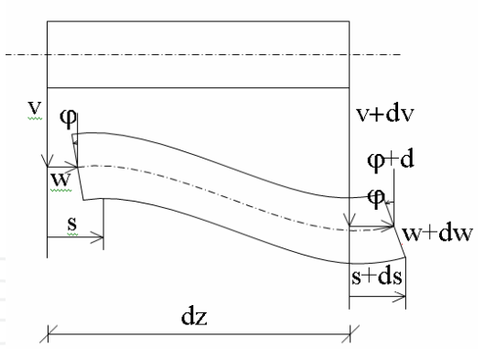

Fig. 3. Displacements components of the segmental element

The interface slip s, namely the axial displacement at the bottom chord of the strip transverse section, can be also related to the displacement components represented in Fig. 3:

$$s = w + \frac{t_f}{2} \cdot \varphi \ . \tag{7}$$

Finally, the usual (generalized) stress-strain relationships can be introduced for the strip modelled as a Bernoulli beam:

$$N = EA_f \varepsilon = E_f b_f t_f \varepsilon \ , \tag{8}$$

$$M = EI_f \chi = E_f \frac{b_f t_f^{\ 3}}{12} \chi \ , \tag{9}$$

where EA_f and EI_f are respectively the axial and flexural stiffnesses which can be assumed for the strip transverse section. Based on the second assumptions reported at the beginning of section 2.1, The following equilibrium equations can be written for the infinitesimal 2D element of resin within the adhesive layer (Fig. 4):

$$\begin{cases} \dfrac{\partial \sigma_{yy}}{\partial y_a} + \dfrac{\partial \tau_{yz}}{\partial z_a} = 0 \\ \dfrac{\partial \tau_{yz}}{\partial y_a} + \dfrac{\partial \sigma_{zz}}{\partial z_a} = 0 \end{cases} , \tag{10}$$

where y_a and z_a are the Cartesian coordinates of the infinitesimal areal element of resin.

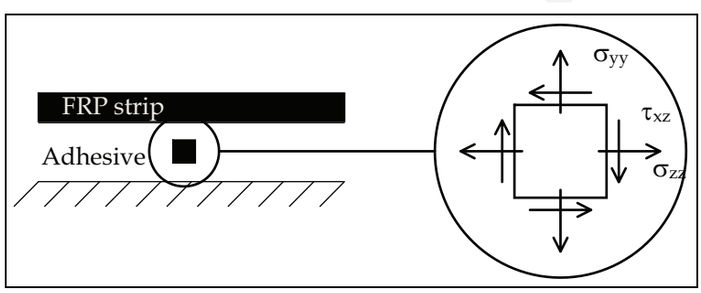

Fig. 4. General plane stress-state for an infinitesimal element of the adhesive layer

The corresponding strain measures can be expressed as functions of the displacement field $v_a(y_a,z_a)$ e $w_a(y_a,z_a)$ within the adhesive layer:

$$\begin{cases} \varepsilon_{yy} = \dfrac{\partial v_a}{\partial y_a} \\ \varepsilon_{zz} = \dfrac{\partial w_a}{\partial z_a} \\ \gamma_{yz} = \dfrac{\partial v_a}{\partial z_a} + \dfrac{\partial w_a}{\partial y_a} \end{cases}, \tag{11}$$

where y_a and z_a are the Cartesian coordinates of the infinitesimal areal element of resin. Finally, the following elastic relationships can be stated between stresses and strains:

$$\begin{cases} \varepsilon_{yy} = \dfrac{1}{E_a} \cdot \left[\sigma_{yy} - \nu_a \cdot \sigma_{zz} \right] \\ \varepsilon_{zz} = \dfrac{1}{E_a} \cdot \left[\sigma_{zz} - \nu_a \cdot \sigma_{yy} \right] \\ \gamma_{yz} = \dfrac{\tau_{xy}}{G_a} = 2 \cdot (1 + \nu_a) \cdot \dfrac{\tau_{xy}}{E_a} \end{cases}, \tag{12}$$

where E_a and G_a are the elastic properties of the adhesive layer. In this formulation, it connects the FRP laminates to a stiff substrate representing the concrete element. The upper bound of this layer is connected to that strip and some compatibility equations should be written for introducing this physical constraint into the mathematical model. Thus, the three equations (10)-(12) can be worked out for deriving a relationship between the displacement components $v_a(0,z_a)$ and $w_a(0,z_a)$ and the corresponding stress components $\sigma_{yy}(0,z_a)$ and $\tau_{xy}(0,z_a)$. A key assumption can be introduced for simplifying the analytical expressions of the interface stresses, considering a constant value of the shear stress throughout the adhesive thickness (Rabinovich & Frostig, 2000):

$$\tau_{yz} = \tau_a(z_a) = \tau_a(z) . \tag{13}$$

Consequently, the second one of the two equations in (10) leads to the following simplification in terms of the normal stress in longitudinal direction:

$$\frac{\partial \sigma_{zz}}{\partial z_a} = 0 \Rightarrow \sigma_{zz} = f_1(y_a) \Rightarrow \sigma_{zz} = 0 . \tag{14}$$

The last implication derives by the assumption of zero axial stress on the initial section of the layer adhesive.

Further simplifications can be introduced looking after the first equations in (10) and introducing therein the stress-strain relationship and the compatibility equation within the adhesive layer:

$$\sigma_{yy}(y_a, z_a) = -\int \frac{d\tau_a}{dz} dy + g_1(z_a) = -\frac{d\tau_a}{dz} y_a + g_1(z_a) , \tag{15}$$

and

$$\varepsilon_{yy}(y_a, z_a) = \frac{\sigma_{yy}(y_a, z_a)}{E_a} = -\frac{1}{E_a} \cdot \frac{d\tau_a}{dz} y_a + \frac{g_1(z_a)}{E_a} . \tag{16}$$

The transverse component of the displacement field can be derived by further integration:

$$\begin{aligned} v_a(y_a, z_a) &= v(z_a) + \int \varepsilon_{yy} dy = v(z_a) + \int \left(-\frac{1}{E_a} \cdot \frac{d\tau_a}{dz} y_a + \frac{g_1(z_a)}{E_a} \right) dy = \\ &= v(z_a) - \frac{1}{E_a} \cdot \frac{d\tau_a}{dz} \frac{y_a^2}{2} + \frac{g_1(z_a)}{E_a} y_a \end{aligned} , \tag{17}$$

and the value of the unknown function g_1 can be finally derived by imposing zero value to the displacement at the bottom interface ($y_a=t_a$):

$$v(z_a) - \frac{1}{E_a} \cdot \frac{d\tau_a}{dz} \frac{t_a^2}{2} + \frac{g_1(z_a)}{E_a} t_a = 0 , \tag{18}$$

$$g_1(z_a) = -\frac{E_a}{t_a} \cdot v(z_a) + \frac{d\tau_a}{dz} \frac{t_a}{2} . \tag{19}$$

Consequently, the following explicit expressions can be written for σ_{yy}, ε_{yy} and v_a described in (15), (16) and (17), by introducing the expression of g_1 given by equation (19):

$$\varepsilon_{yy}(y_a, z_a) = \frac{d\tau_a}{dz} \cdot \left(\frac{t_a - 2y_a}{2 \cdot E_a} \right) - \frac{v(z_a)}{t_a} , \tag{20}$$

$$\sigma_{yy}(y_a, z_a) = E_a \cdot \varepsilon_{yy}(y_a, z_a) = \frac{d\tau_a}{dz} \cdot \left(\frac{t_a - 2y_a}{2} \right) - \frac{E_a}{t_a} v(z_a) , \tag{21}$$

$$v_a(y_a, z_a) = v(z_a) \cdot \left(1 - \frac{y_a}{t_a} \right) + \frac{d\tau_a}{dz} \cdot \left(\frac{t_a - y_a}{2E_a} \right) y_a . \tag{22}$$

Shear strain and stress can be related according to the following relationship:

$$\gamma_{yz}(z_a) = \frac{\tau_a(z_a)}{G_a} , \tag{23}$$

and, considering the compatibility equation involving shear strains, further transformations can be carried out by introducing the compatibility equation in (11):

$$\gamma_{yz}(z_a) = \frac{\partial v_a}{\partial z_a} + \frac{\partial w_a}{\partial y_a} . \tag{24}$$

The first derivative of the longitudinal displacement w_a inside the adhesive layer can be written as follows:

$$\frac{\partial w_a}{\partial y_a} = \gamma_{yz}(z_a) - \frac{\partial v_a}{\partial z_a} = \frac{\tau_a(z_a)}{G_a} - \frac{dv}{dz}\cdot\left(1 - \frac{y_a}{t_a}\right) - \frac{d^2\tau_a}{dz^2}\cdot\left(\frac{t_a - y_a}{2E_a}\right)y_a \ , \tag{25}$$

and the corresponding function w_a can be derived by integrating eq. (25) and introducing a zero-displacement condition for $y_a=t_a$ (namely, at the bottom of the adhesive layer):

$$w_a(y_a, z_a) = -\frac{\tau_a(z_a)}{G_a}(t_a - y_a) + \frac{dv}{dz}\cdot\left(\frac{t_a}{2} - y_a + \frac{y_a^2}{2t_a}\right) + \frac{d^2\tau_a}{dz^2}\cdot\left(\frac{t_a^3}{12E_a} - \frac{t_a y_a^2}{4E_a} + \frac{y_a^3}{6E_a}\right) \ , \tag{26}$$

The above relationship can be utilized for deriving the expression of the axial displacements beneath the laminate ($y_a=0$), corresponding to the slip at the interface s(z):

$$w_a(0, z_a) = s(z) = -\frac{t_a}{G_a}\cdot\tau_a + \frac{t_a^3}{12E_a}\cdot\frac{d^2\tau_a}{dz^2} + \frac{t_a}{2}\cdot\frac{dv}{dz} \ , \tag{27}$$

as well as equation (22) can be utilized for recognizing that the corresponding transverse component $v_a(0,z_a=z)$ is equal to v(z):

$$\sigma_{yy}(y_a, z_a) = E_a\cdot\varepsilon_{yy}(y_a, z_a) = E_a\cdot\left[\frac{d\tau_a}{dz}\cdot\left(\frac{t_a - 2y_a}{2\cdot E_a}\right) - \frac{v(z_a)}{t_a}\right] \ , \tag{28}$$

$$\sigma_y(z) = \sigma_{yy}(0, z_a) = -v(z_a)\cdot\frac{E_a}{t_a} + \frac{t_a}{2}\cdot\frac{d\tau_a}{dz} \ . \tag{29}$$

Thus, the rotation field φ(z) of the laminate element can be easily defined through equation (6) and the generalized strain fields can be determined by means of equation (4) and (5).
The above equations can be finally combined for deriving a unique differential equation in terms of interface shear stresses. A first equation can be obtained by differentiating eq. (7) and introducing (4), (6) and (8). After a further differentiation and introducing the definition of interface slip provided by eq. (27), the following differential relationship between the shear stress and the transverse displacements can be obtained:

$$\frac{G_a}{E_f t_f t_a}\cdot\tau_a - \frac{d^2\tau_a}{dz^2} + \frac{G_a}{2}\cdot\frac{d^3v}{dz^3} + \frac{G_a}{12E_a}\cdot t_a^2\cdot\frac{d^4\tau_a}{dz^4} = 0 \ . \tag{30}$$

Another relationship is obtained by differentiating equation (3) and introducing equation (2), (5), (6) and (9) for expressing both the bending moment and the shear force in terms of transverse displacements and interface (shear and normal) stresses. The final expression of an equation in terms of t_f and v (and their derivatives) can be obtained introducing equation (29):

$$\frac{b_f(t_f + t_a)}{2}\cdot\frac{d\tau_a}{dz} - \frac{E_f b_f t_f^3}{12}\cdot\frac{d^4v}{dz^4} - \frac{E_a b_f}{t_a}\cdot v = 0 \ . \tag{31}$$

The two equations (30) and (31) can be easily combined for deriving the following eighth-order differential equation in terms of interface shear stresses:

$$\frac{G_a}{E_f t_f t_a}\cdot\tau_a-\frac{d^2\tau_a}{dz^2}+\left(\frac{t_a^{\,2}}{3}+\frac{t_a t_f}{6}+\frac{t_f^{\,2}}{12}\right)\cdot\frac{G_a}{E_a}\cdot\frac{d^4\tau_a}{dz^4}-\frac{E_f t_a t_f^{\,3}}{12\cdot E_a}\cdot\frac{d^6\tau_a}{dz^6}+\frac{E_f G_a t_a^{\,3} t_f^{\,3}}{144\cdot E_a^{\,2}}\cdot\frac{d^8\tau_a}{dz^8}=0\,. \quad (32)$$

Finally, an expression of the displacement function v as a function of the interface shear stresses can be derived by solving equation (31) and introducing the (30):

$$v=\frac{3\cdot t_a^{\,2}+3\cdot t_a t_f+t_f^{\,2}}{6E_a}\cdot\frac{d\tau_a}{dz}-\frac{E_f t_a t_f^{\,3}}{6E_a G_a}\cdot\frac{d^3\tau_a}{dz^3}+\frac{E_f t_a^{\,3} t_f^{\,3}}{72\cdot E_a^{\,2}}\cdot\frac{d^5\tau_a}{dz^5}\,. \quad (33)$$

Eight boundary conditions are needed for the problem at hand and they can be symbolically written as follows:

$$\tau_a\big|_{z=0}=0\ ,\ \tau_a\big|_{z=L}=0\ , \quad (34)$$

$$\varepsilon\big|_{z=0}=-\frac{N(0)}{E_f A_f}\ ,\ \varepsilon\big|_{z=L}=\frac{N(L)}{E_f A_f}\ , \quad (35)$$

$$M\big|_{z=0}=0\ ,\ M\big|_{z=L}=0\ , \quad (36)$$

$$V\big|_{z=0}=0\ ,\ V\big|_{z=L}=0\ . \quad (37)$$

Typical solutions of the problem described by equation (32) and the boundary conditions (34)-(37) are represented in figures 5 and 6, in terms of shear and normal stresses respectively. In both graphs, the interface stress components are divided by the average shear stress $\tau_m=F/b_f L$ and the abscissa are reported in non-dimensional form as $\bar{z}=\omega z$.

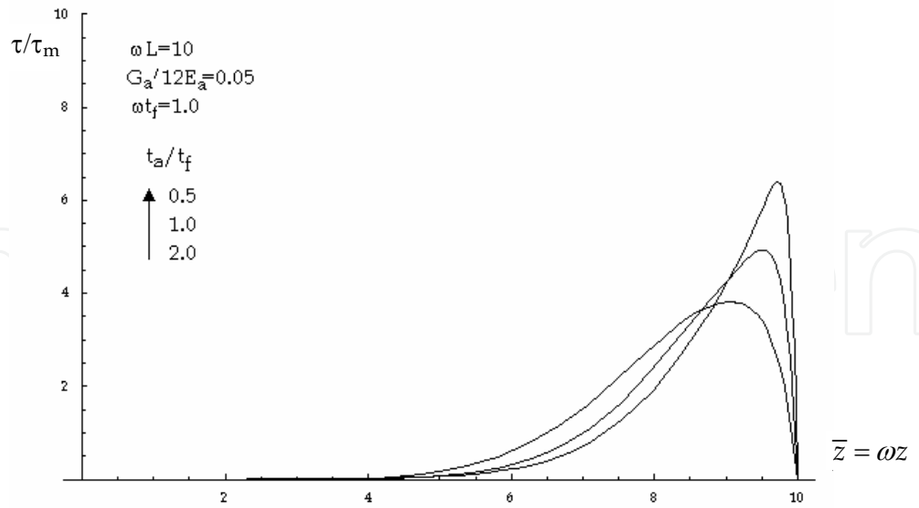

Fig. 5. Possible distributions of interface shear stresses throughout the adhesive interface

The results of the analysis carried out by means of this model are completely controlled by the following non-dimensional parameters:

$$\omega L\ , \quad (38)$$

$$\omega t_f = \sqrt{\frac{G_a t_f}{E_f t_a}} = \sqrt{\frac{k_{s,a} t_f}{E_a}} \ , \tag{39}$$

$$\frac{G_a}{E_a} = \frac{k_{s,a}}{k_{v,a}} \ , \tag{40}$$

$$\frac{t_a}{t_f} . \tag{41}$$

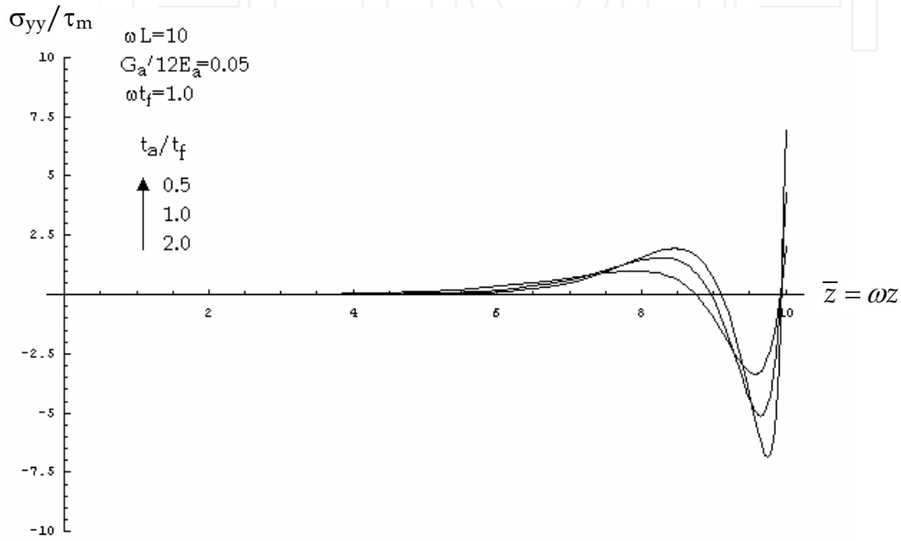

Fig. 6. Possible distributions of interface normal stresses throughout the adhesive interface

2.2 Possible simplifications of the general model

The general model formulated in the previous section can be simplified by introducing further assumptions about the geometric and mechanical assumptions.

In particular, a key simplification derives in the case of negligible thickness t_f of the FRP laminate, if compared, for instance, with a suitable reference value of the length. In particular, it is possible to demonstrate that the height-order equation (32) can be reduced by uncoupling the equations (30) and (31):

$$\frac{d^2\tau_a}{dz^2} + \omega^2 \tau_a = 0 \ , \tag{42}$$

$$\frac{d^4 v}{dz^4} + 12 \cdot \frac{E_a}{t_a t_f^3} v = 0 \ , \tag{43}$$

Under the mathematical point of view, the above simplification derives from the condition $\omega t_f \to 0$ for whichever value of the non dimensional parameters listed at the end of section 2.1. It means that the thickness of the FRP laminate is much smaller than the characteristic length of the problem ω, which is the main argument of the solutions of the general equation (32). The uncoupled boundary conditions for eq. (42) simplify as a consequence of the condition $\omega t_f \to 0$, turning in a completely uncoupled expressions:

$$\varepsilon\big|_{z=0} = -\frac{N(0)}{E_f b_f t_f} = \left.\frac{ds}{dz}\right|_{z=0} \quad \varepsilon\big|_{z=L} = \frac{N(L)}{E_f b_f t_f} = \left.\frac{ds}{dz}\right|_{z=L} . \tag{44}$$

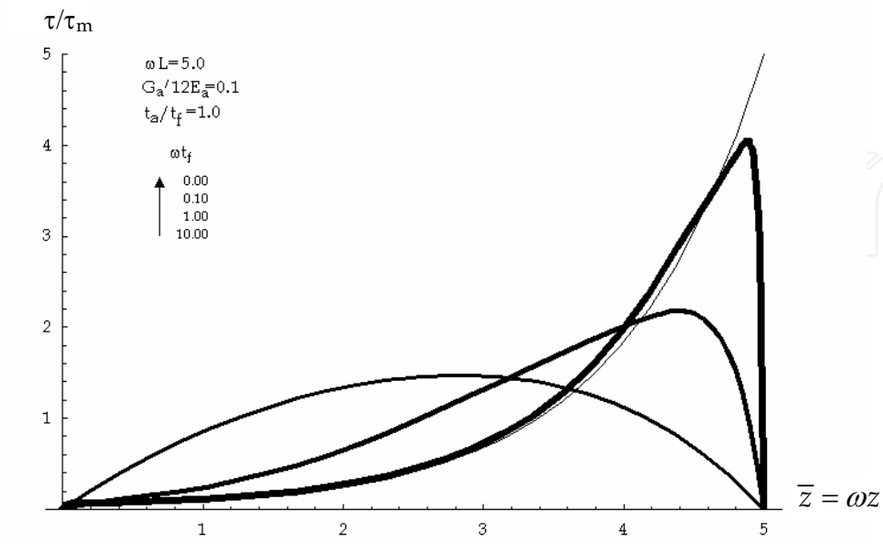

Fig. 7. Interface shear stress for a thin FRP strip

A sound demonstration about how equation (32) reduces to (42)-(43) in the case of $\omega t_f \to 0$, can be obtained by means of some mathematical transformations of both the equation (32) and the boundary conditions (34)-(37) in dimensionless form. These transformations, as well as the discussion about the slight modifications in the out-of-plane stress regime, are omitted herein for the sake of brevity.

2.3 Solutions in the nonlinear range

The assumption introduced in the subsection 2.2 for simplifying the general eighth-order equation formulated in subsection 2.1 can be generally assumed as a reasonable trade-off between the (good) accuracy of the obtained model and the (higher) simplicity of its equations. The approximation introduced by the supplementary assumption is generally accepted especially in the nonlinear range, as further uncertainties are introduced by the fracture behaviour of concrete which cannot be covered by the complex assumptions leading to equation (32).

Thus, the nonlinear response of FRP-to-concrete joints under pull-out actions can be analyzed by assuming the problem described by equation (42) with the boundary conditions in (44). Since the nonlinear response is now of interest, equation (42) can be slightly modified for considering the possibility of a nonlinear relationship $\tau_a=\tau(s)$. Moreover, eq. (1) can be written in terms of axial strains ε in the FRP strip by introducing equation (8):

$$\frac{d\varepsilon}{dz} + \frac{\tau(s)}{E_f t_f} = 0 \ . \tag{45}$$

and, considering the relationship between axial strains and interface slip derived at the end of the subsection 2.2, the following relationship can be written for generalizing eq. (42) to the nonlinear range:

$$\frac{d^2s}{dz^2}+\frac{\tau(s)}{E_f t_f}=0 \ . \tag{46}$$

The bilinear shear-stress-interface-slip relationship is considered herein as a general relationship for the nonlinear response of the interface between FRP and concrete:

$$\tau(s)=\begin{cases}-k_{el}\cdot s & |s|\le s_{el}\\ -k_u\cdot(s_u-|s|)\cdot \mathrm{sign}(s) & s_{el}<|s|\le s_u\\ 0 & |s|>s_u\end{cases}, \tag{47}$$

where all symbols are represented in Fig. 8. For the sake of simplicity, only the monotonic behaviour with s≥0 will be considered in the following elaborations.

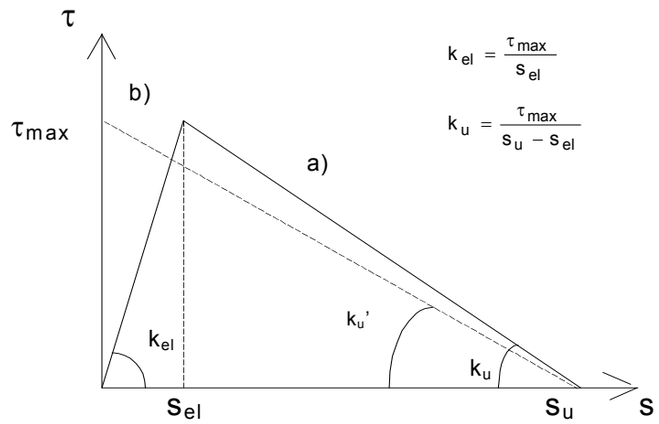

Fig. 8. Bilinear shear-stress-interface-slip relationship (fib - bulletin 14, 2001)

Consequently, two second order differential equations can be obtained by introducing the two nonzero branches of the relationship (47) within the general equation (46). In particular, under low load levels, the condition $0\le s\le s_{el}$ yields throughout all the bonding length and the equation (46) can be written in the following form in terms of interface slips s:

$$\frac{d^2s}{dz^2}-\omega^2\cdot s=0 \ . \tag{48}$$

Considering a pull-out force P applied at the end (z=L) of the bonding length, the following boundary conditions can be written after eq. (44):

$$\varepsilon\big|_{z=0}=\left.\frac{ds}{dz}\right|_{z=0}=0 \qquad \varepsilon\big|_{z=L}=\left.\frac{ds}{dz}\right|_{z=L}=\frac{P}{E_f b_f t_f} \ . \tag{49}$$

Simple mathematical transformations (whose details are omitted herein) lead to the following solution in terms of interface shear stresses

$$\tau=-\omega\cdot\frac{P}{b_f}\cdot\frac{\cosh(\omega\cdot z)}{\sinh(\omega L)} \ , \tag{50}$$

which can be easily turned in terms of interface slips s considering the expression describing the linear elastic branch in eq. (47). This solution can be accepted for values of the shear strength $|\tau| \le \tau_{max}$ or, in order words, for pull-out forces lower than P_{el}:

$$F_{el} = \frac{\tau_{max}}{\omega} \cdot b_f \ . \tag{51}$$

leading to an interface slip $s=s_{el}$ in $z=L$. As $P>P_{el}$, two different parts of the adhesive interface can be recognized. In the first part, namely for $0 \le z \le z_{el} < L$, the values of the interface slips s keep smaller than the elastic threshold s_{el}. In the second part, for $z_{el} < z \le L$, the interface slips s are in the range (s_{el}, s_u), and the following solution can be derived by integrating the two differential equations:

$$\frac{d^2 s_1}{dz^2} - \omega \cdot s_1 = 0 \quad \text{for} \quad 0 \le z \le z_{el} < L, \tag{52}$$

$$\frac{d^2 s_2}{dz^2} + \frac{k_{in}}{E_f t_f} \cdot s_2 = \frac{k_{in}}{E_f t_f} \cdot s_u \quad \text{for} \quad z_{el} < z \le L. \tag{53}$$

with the following boundary conditions:

$$\varepsilon\big|_{z=0} = \left.\frac{ds_1}{dz}\right|_{z=0} = 0 \qquad s_1\big|_{z=z_{el}} = s_{el} \tag{54}$$

$$s_1\big|_{z=z_{el}} = s_1\big|_{z=z_{el}} \qquad \left.\frac{ds_1}{dz}\right|_{z=z_{el}} = \left.\frac{ds_2}{dz}\right|_{z=z_{el}} \tag{55}$$

The following solution in terms of interface shear stress τ involves the parameter $z_{el} < L$, describing the length of the elastic part of the bonding length:

$$|\tau| = \begin{cases} \tau_{max} \dfrac{\cosh(\omega \cdot z)}{\cosh(\omega \cdot z_{el})} & 0 \le z \le z_{el} \\ \tau_{max} \left\{ \cos\left[\omega_{in}(z - z_{el})\right] - \dfrac{\omega_{in}}{\omega} \cdot \sin\left[\omega_{in}(z - z_{el})\right] \cdot \tanh(\omega z_{el}) \right\} & z_{el} < z \le L \end{cases} \tag{56}$$

where

$$\omega_{in} = \sqrt{\frac{\tau_{max} / (s_u - s_{el})}{E_f t_f}} = \sqrt{\frac{k_{in}}{E_f t_f}} \ . \tag{57}$$

Fig. 9 shows two typical distributions of shear stresses in the a) linear and b) nonlinear range of the behaviour of the adhesive interface described by the bilinear relationship in eq. (47).
It is worth noting that z_{el} can actually range in the interval $[z_{el,min}, L)$:

$$z_{el,min} = \max\{0; z_{el,deb}\} \tag{58}$$

in which $z_{el,deb}$ is the value of z_{el} leading to $\tau(L)=0$ (or $s(L)=s_u$):

$$\cos\left[\omega_{in}\left(L-z_{el,deb}\right)\right]-\sqrt{\frac{k_{in}}{k}}\cdot\sin\left[\omega_{in}\left(L-z_{el,deb}\right)\right]\cdot\tanh\left(\omega\cdot z_{el,deb}\right)=0\,. \tag{59}$$

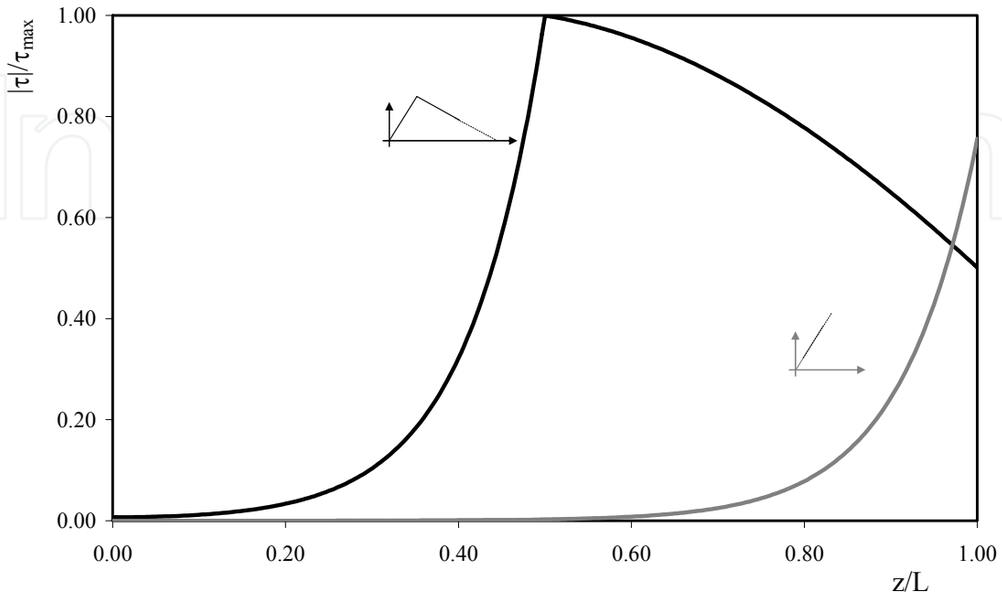

Fig. 9. Typical distribution of interface shear-strength in the linear and nonlinear range

2.4 Key parameters related to the ultimate strength

The case of $z_{el,deb}=0$ is of particular relevance, as it represents the condition of debonding initiation (namely, $s(L)=s_u$) with $\tau(0)=\tau_{max}$. A characteristic length L_{eff} can be defined in that case by means of equation (59):

$$\cos\left[\omega_{in}L_{eff}\right]=0\;\Rightarrow\;L_{eff}=\frac{\pi}{2}\cdot\sqrt{\frac{E_f t_f}{k_{in}}}\;. \tag{60}$$

Under the mechanical standpoint, this characteristic value has a paramount conceptual meaning. It represents the border between "short" and "long" anchorage length. In particular, the general expression of the force $F>F_{el}$ corresponding to a given position of z_{el} can be derived by integrating the shear stresses in equation (56):

$$F=\tau_{max}b_f\cdot\left\{\frac{\sin\omega_{in}\left(L-z_{el}\right)}{\omega_{in}}+\frac{\cos\omega_{in}\left(L-z_{el}\right)\cdot\tanh\omega z_{el}}{\omega}\right\}. \tag{61}$$

It can be applied if and only if $z_{el}\in[z_{el,min}, L)$ (namely, the interface slip s is $s_{el}\le s\le s_u$). In the case of $z_{el}=L$ equation (61) reduces to (51). On the contrary, when $z_{el}=z_{el,deb}=0$ the following expression can be derived for the pull-out force:

$$F_{deb}=\tau_{max}b_f\cdot\frac{\sin\omega_{in}L_{eff}}{\omega_{in}}=\frac{\tau_{max}b_f}{\omega_{in}}=b_f\cdot\sqrt{\tau_{max}\cdot\left(s_u-s_{el}\right)\cdot E_f t_f}\;. \tag{62}$$

Since generally $s_u >> s_e$ the value F_{deb} is only slightly lower than the maximum strength F_{max} which can be evaluated by applying the theory of Fracture Mechanics (Täljsten, 1996) (or either as a maximum on z_{el} of the for F in eq. (61)):

$$F_{max} = b_f \cdot \sqrt{2G_F \cdot E_f t_f} = b_f \cdot \sqrt{\tau_{max} \cdot s_u \cdot E_f t_f} \quad . \tag{63}$$

They can be assumed as coincident in the approximation of rigid-softening behaviour in considered Fig. 9.
Note that equation (63) can be applied only if $L_b \geq L_{eff}$ being L_{eff}, the effective transfer length. If $L_b < L_{eff}$ a smaller value of the ultimate force has to be expected according to the following relationship:

$$F_{max} = \sqrt{2G_F E_f t_f} \cdot b_f \cdot \left[\frac{L_b}{L_{eff}} \cdot \left(2 - \frac{L_b}{L_{eff}} \right) \right]. \tag{64}$$

3. Experimental testing techniques and results

As stated above, the effectiveness of FRP externally bonded on RC members is strongly related to the interface behaviour that depends on the mechanical and geometrical properties of materials. Thus an FRP-to-concrete bond strength model is the key to the accurate prediction of debonding failures in FRP-strengthened RC beams, including plate end debonding failures and shear crack-induced debonding failures, as well as intermediate flexural or flexural-shear crack-induced debonding failures (Teng et al., 2002).
Plenty of pull-out tests have been carried out by researchers during last years in order to experimentally investigate the influence of FRP and concrete mechanical properties on the bonding behaviour.
An overview of most common bond test techniques is reported in the first subsection. Then, the most significant results achieved by such bond tests are showed in the second one.

3.1 Overview of testing techniques

Yao et al. (2005) classified the existing test setups into the following types: (a) double-shear pull tests; (b) double-shear push tests; (c) single-shear pull tests; (d) single-shear push tests; and (e) beam (or bending) tests. These arrangements are based on the definition of the loading condition of the element and on the symmetry of the system (a double or single test refers to the contemporaneous loading of two or one FRP reinforcement applied on the specimen sides). Collectively, the first four test methods, may also be referred to as pull tests, as the plate is always directly pulled by a tensile force. Pull-pull (a) and push-pull (d) test setup are the most popular test methods. In end debonding failures in FRP flexural- strengthened RC beams with longitudinal laminates as well as debonding failures in FRP shear-strengthened RC beams with transverse laminates, the bond strength model developed from pull tests is directly applicable. Furthermore, in intermediate crack-induced debonding failures in FRP flexural- strengthened RC beams with longitudinal laminates, the stress state in the critical region of the beam is also closely similar to that of the concrete prism in a single-shear pull test. In order to extend the results of bond tests to various types of strengthening (flexural, shear, torsion), the pull-pull test setup (a and c) are probably the configuration giving the loading condition more similar to the actual one in RC elements, but it is also the most difficult to realize with a reliable setup. Furthermore the test setup (a), as well as (b) could lead to

underestimate the bond strength due to the influence of detailing (Blontrock et al., 2002; Ceroni et al., 2008). On the contrary, the push-pull test (d), where the concrete is partially in compression, is easier to be realized but it gives comparable predictions of the bond strength, if the pushing force is applied on the concrete block sufficiently far from the external reinforcement (Yao et al., 2005). Indeed, if the compressed area of concrete is too extended, the volume of material involved in the debonding failure can be lower and, thus, the related fracture energy decreases.
Asymmetrical schemes (c and d) are, in general, preferable to the symmetrical ones (a and b) mainly because the latter are more influenced by the alignment detailing of the two strengthened sides. Moreover the specimen symmetry is however lost when the debonding starts on one side and prevents from following correctly the post-peak behaviour.
As concerns the asymmetrical push-pull test setups (d), they are commonly realized by positioning a single concrete block in a stiff steel frame with an upper plate compressing the specimen, while the end of the FRP reinforcement, glued on one side, is clamped in the grips of a tensile machine (Nigro et al., 2008; Savoia et al. 2009; Ceroni and Pecce, 2010). An alternative configuration can be also realized by fixing the end of the concrete block, placed horizontally, and applying tension to the FRP reinforcement with an hydraulic jack (Yao et al., 2005; Mazzotti et al., 2009). As concerns the asymmetrical pull-pull test setups (c), they can be realizes by installing metallic threaded rods inside the concrete specimen which can be clamped in the testing machine grips (Bilotta et al. 2011).
Asymmetrical single-shear test setup (c or d) appear to be promising candidate as a standard setup for determining the FRP-to-concrete bond strength; hence they were adopted to perform the tests showed in the following section.

3.2 Experimental results

A total of 58 SST tests in four sets (i.e. I-12 tests, II-16 tests, III-12 tests, IV-18 tests) were performed on CFRP plates (38) and sheets (20) applied on two opposite longitudinal faces of 29 concrete prisms. Concrete mix was specifically designed to obtain low compressive concrete strength to simulate the FRP application on existing concrete. Compressive tests were performed at 28 days after casting: the cylinder mean strength, f_{cm}, was equal to 23.82 MPa, 21.46 MPa, 26.00 MPa and 19.00 MPa for set I, II, III and IV respectively. CFRP Young's moduli, E_f, were obtained by means of tensile flat coupon tests: their mean values were between 110-220 GPa for plates and 170-240 GPa for sheets. Prior to FRP installation, the concrete surface was treated by sand paper (sets I, II, III) or by bush hammering (set IV), in order to eliminate the mortar till the aggregate became clear. Primer was always used to consolidate the concrete surface except for specimens of set VI. Further details related to experimental tests of each set can be founded in (Nigro et al. 2008, Savoia et al. 2009, Bilotta et al. 2009, Bilotta et al. 2011).
Note that several strain gauges were applied along the FRP laminates in order to measure axial strains during the bond test (see Fig. 10b,c). Experimental readings allow theoretical models of the adhesion laws to be to verified or calibrated.
The behaviour of the FRP-to-concrete interface was analyzed by plotting the experimental axial strains $\varepsilon_i(z)$ measured by means of strain gauges during the test along the FRP reinforcement. Strains recorded along FRP plates at different load level are plotted in Fig. 12a,b for sheets and plates respectively. The first debonding load, P_{fd}, identified the beginning of debonding.

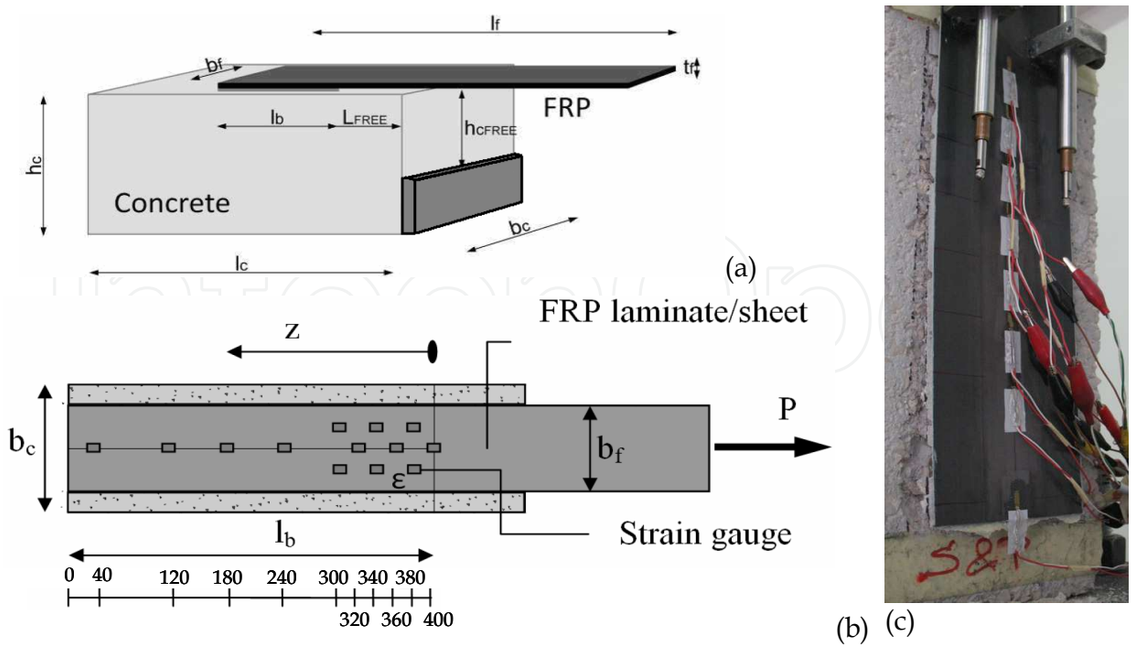

Fig. 10. Test setup scheme (a) – strain gauges distributions: scheme (b) and photo (c)

Fig. 11. Specimen after test and typical failure mode

Note that the maximum strain recorded at the loaded ends of FRP sheets was $\varepsilon_{sheets} \approx 0.6\%$; for plates it was significantly lower ($\varepsilon_{plates} \approx 0.2\%$), even if, for both types of reinforcement, the bond length was higher than the theoretical effective one, $L_{eff} = \sqrt{(E_f \cdot t_f)/(2 \cdot f_{ctm})}$, evaluated according to *fib* bulletin 14 (2001) and CNR-DT200/2004 (2004), where f_{ctm} is the mean tensile strength. Such result is mainly due to the higher stiffness of plates; indeed, as showed above by (63), the FRP stiffness, $E_f t_f$, is the main parameter affecting the debonding strain, being maximum strain at debonding phenomenon being the maximum strain due to debonding proportional to the factor $\sqrt{1/(E_f t_f)}$. In particular, the ratio $\left(\sqrt{1/(E_f t_f)}\right)_{sheets} / \left(\sqrt{1/(E_f t_f)}\right)_{plates}$ of FRP reinforcements investigated in Fig. 12 is 2.5

similar to $\varepsilon_{sheets} / \varepsilon_{plates} \approx 3$. Moreover, since plates are about eight times thicker than sheets while the ratio between Young moduli is very close to unity (i.e. $E_{f,S}/E_{f,P}=1.35$), this result seems to confirm that the reinforcement thickness particularly affects debonding behaviour. Indeed, the greater the thickness, the higher the increase in the normal and shear stresses at FRP to concrete interface and consequently the probability of premature debonding occurrence (Oehlers and Moran, 1990; Tounsi et al., 2009).

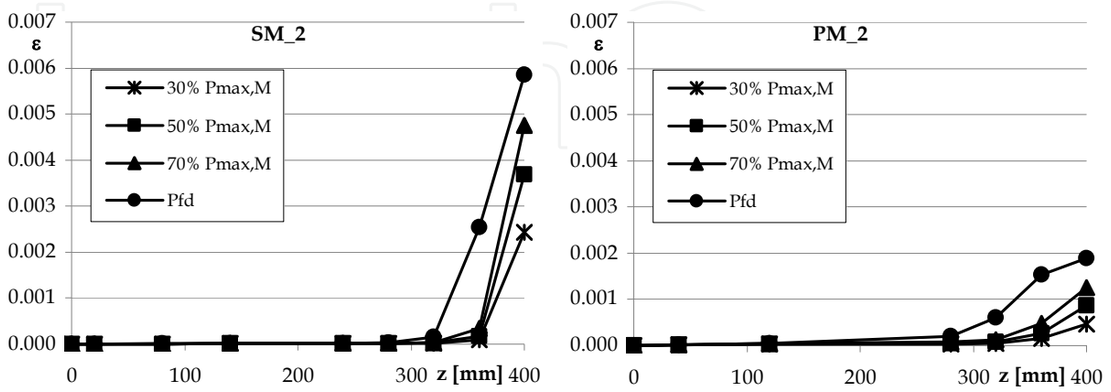

Fig. 12. Strain recorded on sheet (a) and plate (b) reinforced specimens

The interface shear stresses $\tau_i(z)$ were obtained by the variation of axial stress and, hence, strain throughout the FRP by the following relationship between two strain gauges at distance $\Delta z_{i,i+1}$

$$\tau_{i,i+1} = \frac{\varepsilon_{i+1} - \varepsilon_i}{\Delta z_{i,i+1}} \cdot E_f \cdot t_f \tag{65}$$

where E_f and t_f are FRP Young's modulus and thickness, respectively. Typical shear stress profiles assessed for sheets and plates, respectively, are reported in Fig. 13a,b.
Note that, at the loaded end of the reinforcement, the shear stresses assessed for loads close to the debonding of the reinforcement are lower than those assessed for lower loads. This indicates that in this zone of the reinforcement the shear-stress-slip law is in the softening stage typical of a post-elastic behaviour.

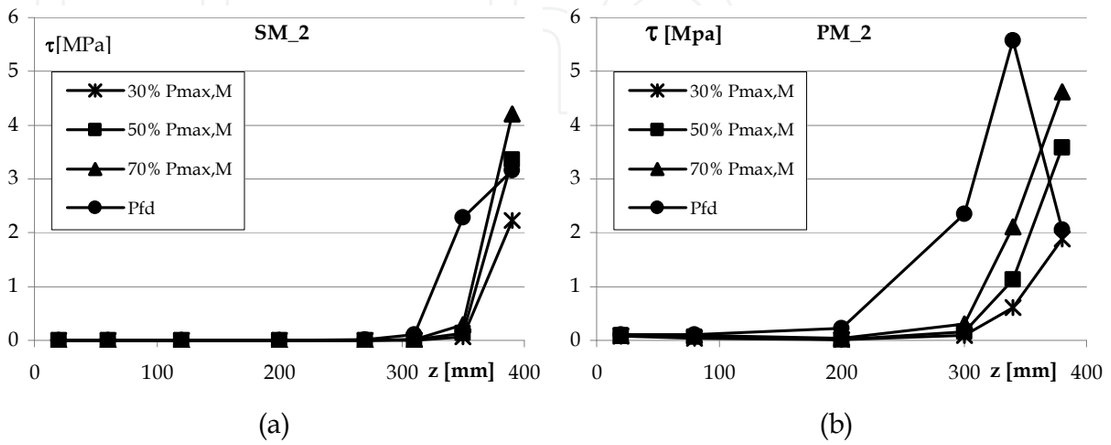

Fig. 13. Shear stresses assessed on sheet (a) and plate (b) reinforced specimens

The shear-stress-slip relationship, describing the FRP-to-concrete interface law, can be identified starting from the experimental results of pull-out tests; the distribution of shear stresses could be, in fact, obtained by Eq. (65) and the corresponding slips values by integrating the axial strains measured during the test by the following relationship

$$s_{i,i+1} = \sum_{k=0}^{i} \frac{(\varepsilon_{k+1} + \varepsilon_k)}{2} \cdot (x_{k+1} - x_k) \tag{66}$$

In particular the bond law at the FRP-to-concrete interface (see Fig. 14) can be obtained by calculating the shear stresses using Eq. (65) (considering the strains recorded by two gauges nearest the loaded end of FRP, see Fig. 10) and the corresponding slips using Eq. (66) (considering all the strain gauges applied on the FRP reinforcement).

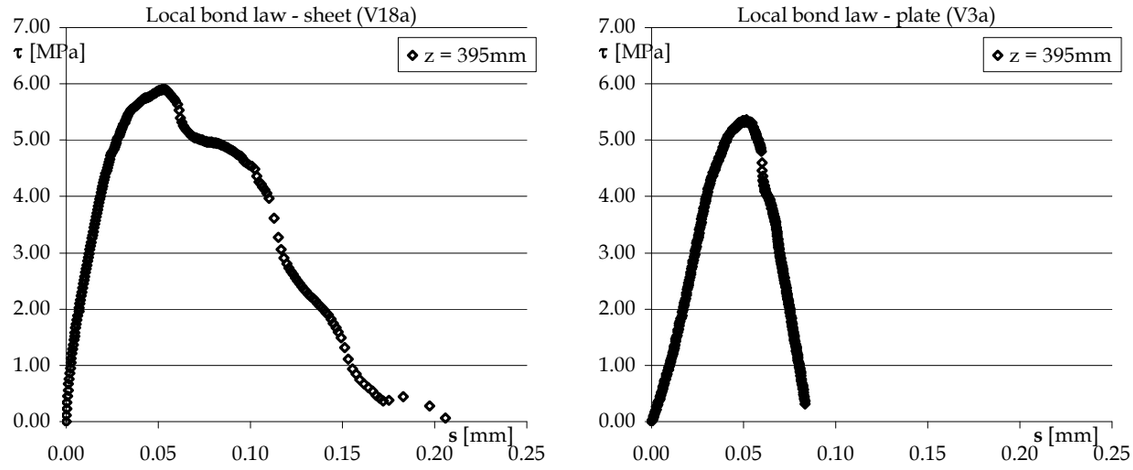

(a) (b)

Fig. 14. Experimental bond law at the FRP-to-concrete interface: sheet (a) and plate (b)

In this way a direct identification method (DirIM) is put in place since the interface law is obtained directly with respect to experimental values of shear stresses and relative slips.

As stated above, according to the study made by Taljsten (1996), derived by linear fracture mechanics, the maximum value F_{max} of the force applied to the FRP-to-concrete joint can be obtained by (63) where G_F is the specific fracture energy of the interface depending on the mechanical properties of the adhesive FRP-to-concrete interface.

Although plenty of alternative models are available in the literature (i.e. Savoia et al., 2003) to describe FRP-to-concrete interface interaction, a simplified bi-linear relationship can reproduce the key aspects of the interface behaviour as pointed out by the comparative study carried out by Lu et al. (2005). Elasto-softening bilinear relationship is one of the most widely accepted expressions for the interface relationship and fracture energy; three mechanical parameters completely identifies such relationship (maximum shear stress τ_{max}, ultimate slip s_u, and elastic stiffness k_e), but obviously the knowledge of G_F by solving equations (63) and (64), is not sufficient for determining such parameters.

As widely discussed in Faella et al. (2009), two approaches are mainly possible to calibrate an interface relationship: the first approach (Direct Identification Method - DirIM) starts

from the experimental strains measured during the test: the distribution of shear stresses can be roughly evaluated through equilibrium of the axial stresses depending on the axial strain by (65); the corresponding slip values can be obtained by integrating throughout the FRP the axial strains by (66). The couples of values $\left(\overline{s}_j, \overline{\tau}_j\right)$ can be "directly" used to calibrate the τ-s relationship through a numerical regression, such as the least square method. Although the DirIM is very easy under the analytical standpoint, the drawback of the method is that the distribution of shear stresses cannot be directly compared with data provided by the pull out tests, because both interface shear stresses and local displacements cannot be directly measured during the usual pull-out tests. In order to overcome such problem, the indirect identification procedure (IndIM) can be pursued to calibrate an interface relationship starting from the availability of axial strain evolution in FRP plate at different load levels up to debonding failure: once a bi-linear interface relationship has been assigned, the corresponding theoretical strain distributions can be evaluated and compared with experimental data; the procedure is iterative and ends when the difference between theoretical and experimental strains is less than a prefixed tolerance (Faella et al., 2003).
With reference to some experimental data (Nigro et al., 2008) both DirIM and IndIM have been applied in order to plot the τ-s relationship and derive the corresponding specific fracture energy G_F, computed by totalling up the area under the bi-linear curve.
Table 1 shows that IndIM leads to specific fracture energy G_F larger than those computed by DirIM in almost all analyzed cases. Moreover, in the case of experimental tests carried out by the authors, values of G_F obtained with IndIM are as stable as the measured failure loads P_{test}, confirming the superior accuracy of IndIM with respect to DirIM. Some of the most representative bi-linear interface relationships obtained by applying both DirIM and IndIM are reported in Fig. 15.

Label		**PM_1**	**PM_2**	**PM_3**	**SM_1**	**SM_2**	**SM_3**
$\mathbf{G_F}$	(DirIM)	0.45	1.20	0.86	0.66	0.86	0.48
$\mathbf{G_F}$	(IndIM)	0.73	1.75	1.03	0.66	0.67	0.72
$\mathbf{G_{F,(IndIM)}/G_{F,(DirIM)}}$		1.61	1.46	1.20	0.99	0.78	1.50

Table 1. Specific fracture energy GF: (DirIM) Vs (IndIM)

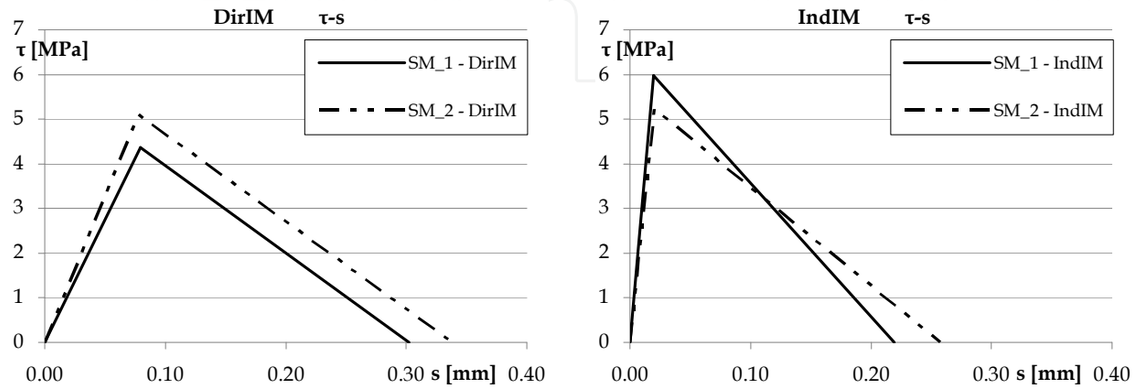

Fig. 15. Bi-linear interface relationship: (DirIM) Vs (IndIM)

Two methods lead to results that could be even significantly different, especially in terms of ultimate slips. Furthermore, the ascending branches of DirIM curves are characterized by a lower slope with respect to IndIM.
Comparisons between the theoretical and experimental values of the axial strains throughout the FRP plate are reported, for different values of load test, in Fig. 16. The results are referred to test SM_3. The theoretical strain values have been obtained by closed-form solutions reported in Faella et al. (2003).

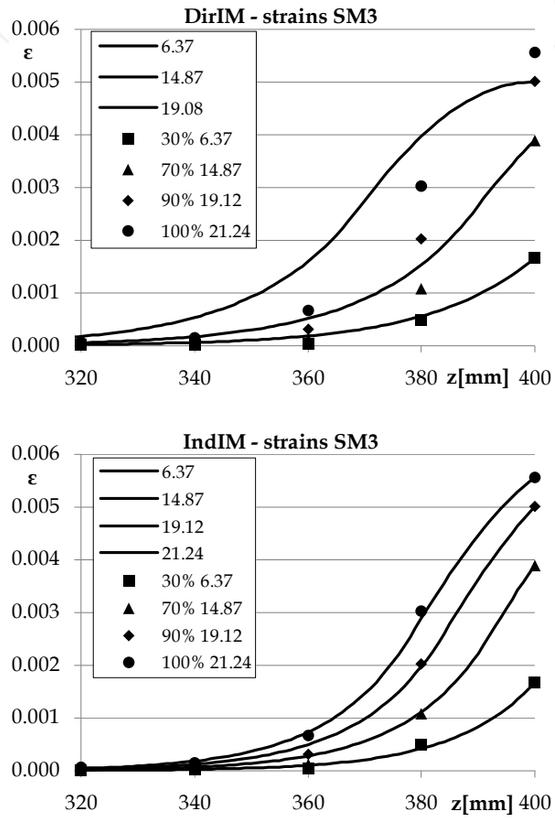

Fig. 16. Theoretical and experimental strains: (DirIM) Vs (IndIM)

The theoretical values of strains obtained assuming the interface relationship identified through IndIM are much closer to the observed ones than the values which can be derived assuming the τ-s relationship calibrated by means of DirIM. Finally it is worth observing that the experimental data can be simulated with good accuracy even if a simplified adhesion law (i.e. a bilinear adhesion law) is assumed.

4. Design formulae

The fracture energy, Γ_F, depends on both the strength properties of adherents, concrete and adhesive, and the properties of the concrete surface. When the reinforcement is correctly applied, the detachment of the reinforcement occurs with debonding in the concrete layer and the specific fracture energy of the interface law can be written in a form similar to that

used for the shear fracture (mode I). Therefore, in order to obtain design formulae, the fracture energy can be expressed as a function of the shear strength in the concrete: $\Gamma_F(\tau_{b,max})$, where $\tau_{b,max}$ depends on the tensile and compressive strength of concrete.

4.1 Theoretical formulations of debonding load

In most formulations the fracture energy is directly expressed as function of the tensile and/or compressive strength of concrete and it is also function of a shape factor depending on the FRP to concrete width (b_f/b_c).

Based on experimental tests, many theoretical formulations have been proposed in the past (Taljsten, 1994; Neubauer and Rostasy, 1997; Brosens and Van Gemert, 1997; fib bulletin, 2001; Chen and Teng, 2001; Smith and Teng, 2002; CNR-DT200, 2004; Lu et al., 2005; Seracino et al., 2007) to evaluate bond strength at the end of R.C. beams externally strengthened with FRP.

The lay out of the existing formulations is often similar; the differences are essentially related to the numerical coefficients calibrated on experimental results and to the eventual presence of safety factors. This last point is an important issue in using these formulations for design when the safety level (mean, characteristic or design provisions) has to be chosen. Some of these formulas are used to predict the bond strength at the intermediate crack too, through the exchange of some factors (Teng et al., 2003; Chen et al., 2006; CNR-DT200, 2004). For illustrative purposes an example of a calibration procedure of a simplified design relationship based on experimental data is reported in the following section. The example was made with reference to the theoretical relationship (67) suggested in CNR DT200-2004 but the procedure can be used to calibrate also different formulations.

$$N_{f,max} = \frac{1}{\gamma_{f,d}\sqrt{\gamma_c}} \cdot \beta_L \cdot b_f \cdot \sqrt{k_G \cdot k_b} \sqrt{2 \cdot E_f \cdot t_f \cdot \sqrt{f_{ck} \cdot f_{ctm}}} \tag{67}$$

$$L_e = \sqrt{\frac{E_f \cdot t_f}{2 \cdot f_{ctm}}} \tag{68}$$

$$k_b = \sqrt{\frac{2 - b_f/b_c}{1 + b_f/400}} \tag{69}$$

$$\beta_l = \frac{L_b}{L_e} \cdot \left(2 - \frac{L_b}{L_e}\right) \quad \text{if} \quad L_b \le L_e; \qquad \beta_l = 1 \quad \text{otherwise} \tag{70}$$

f_{ck} being the characteristic value of cylindrical compressive strength of concrete, k_G a coefficient regarding the experimentally calibrated fracture energy and equal to 0.064 for mean value provision or 0.03 for design value. The safety factor for debonding failure, $\gamma_{f,d}$, is usually assumed equal to 1.2 or 1.5 (non-controlled or controlled gluing application); γ_c is the safety factor for concrete (equal to 1.5, EC2, 2004).

4.2 Simplified calibrating procedure

The mean value of the maximum axial strain in FRP corresponding to debonding failure can be expressed by means of a relationship obtained by a deterministic model and fine-tuned

on experimental data through a probabilistic approach, as suggested in (EN1990 – Annex D) and applied by Monti et Al. (2009).
By assuming a simplified formulation similar to the design relationship (67), taking into account no safety partial factors, the debonding strain can be expressed as:

$$\varepsilon_{fd}\left(k_{bf},f_c,f_{ct},E_f,t_f,b_f,k_b\right)=k_{bf}\cdot\sqrt{\frac{2\cdot k_b\cdot\sqrt{f_c\cdot f_{ct}}}{E_f t_f}} \tag{71}$$

where the coefficient k_{bf} can be calibrated based on experimental results using a least-square procedure consisting in the resolution of the following minimum problem (Bilotta et al. 2011):

$$k_{bf}=\arg\min_{k_{bf}}\sum_{i=1}^{n}\left[\varepsilon_{fd}\left(k_{bf},f^{(i)},f_{ct}^{(i)},E_f^{(i)},t_f^{(i)},b_f^{(i)},k_b^{(i)}\right)-\varepsilon_{exp}^{(i)}\right]^2 . \tag{72}$$

Furthermore, a random variable δ can be defined, for each ith test, as the ratio of the experimental debonding strain, $\varepsilon_{exp,i}$, to the theoretical one, $\varepsilon_{fd,i}$, evaluated by considering the geometric and mechanical data characterizing that test:

$$\delta_i=\frac{\varepsilon_{exp,i}}{\varepsilon_{fd,i}} . \tag{73}$$

The error function, δ, can cover the uncertainties of the simplified model considered as follows:

$$\varepsilon_{fd}=\varepsilon_{fd}\left(k_{bf},f_c,f_{ct},E_f,t_f,b_f,k_b\right)\cdot\delta , \tag{74}$$

therefore, the mean value of the intermediate debonding strain can be obtained by a coefficient k_m, starting from k_{bf} adjusted by means of the mean value of the error parameter $\overline{\delta}$, being in general $\overline{\delta}\neq 1$ because the regression line is imposed to intercept the origin:

$$k_m=k_{bf}\cdot\overline{\delta} . \tag{75}$$

Obviously, this strain is proportional to the debonding stress, being linear elastic the FRP constitutive law.
If the random variable represents a strength, its characteristic value is often defined for design purposes as the 0.05 percentile of the frequency distribution associated to the examined variable. Gauss distribution is the most generally considered for describing the errors. Assuming that the Young modulus of the FRP reinforcement, E_f, and the concrete tensile and compressive strengths, f_{ctm} and f_{cm}, are the only mechanical parameters influencing the value of the maximum axial strain developed in FRP at debonding, the expressions for the both general model and the calibrated one involving the coefficient k_{bf} as well as $\overline{\delta}$ are:

$$\varepsilon_{th}=\varepsilon_{th}\left(E_f,f_{cm,}f_{ctm}\right) , \tag{76}$$

$$\varepsilon_{th,m} = \varepsilon_{th,m}\left(E_f, f_{cm,} f_{ctm}, \bar{\delta}, k_{bf}\right). \tag{77}$$

E_f, f_c and f_{ct} are assumed normally and independently distributed random variables, with a priori values of the coefficients of variation according to the design relationships provided by codes and literature information (Bilotta et al. 2011). Also the variable δ can be assumed as normally distributed. However, the hypothesis of normal distribution is required to be checked at least by comparing the experimental curve of the cumulative frequency to the theoretical one corresponding to a Gaussian distribution having the same mean value and standard deviation. Hence, under the hypothesis of normal distribution for the variable δ, the strain provision corresponding to the 0.05 percentile of the Gaussian distribution is:

$$\varepsilon_{th,k} = \varepsilon_{th,m} - 1.64 \cdot \left[\mathrm{Var}(\varepsilon_{th,m})\right]^{0.5} \tag{78}$$

where the variance of $\varepsilon_{th,m}$ can be expressed as:

$$\mathrm{Var}\left(\varepsilon_{th,m}\right) = C_{Efm}^2 \cdot \mathrm{Var}\left(E_f\right) + C_{fcm}^2 \cdot \mathrm{Var}\left(f_{cm}\right) + C_{fctm}^2 \cdot \mathrm{Var}\left(f_{ctm}\right) + C_{\delta m}^2 \cdot \mathrm{Var}\left(\delta_m\right) \tag{79}$$

$$C_{Efm} = \left|\frac{\partial \varepsilon_{th,m}}{\partial E_f}\right|_{\overline{E_f}},\ C_{f_{cm}} = \left|\frac{\partial \varepsilon_{th,m}}{\partial f_{cm}}\right|_{\overline{f_{cm}}},\ C_{f_{ctm}} = \left|\frac{\partial \varepsilon_{th,m}}{\partial f_{ctm}}\right|_{\overline{f_{ctm}}},\ C_{f_{ctm}} = \left|\frac{\partial \varepsilon_{th,m}}{\partial \delta_m}\right|_{\overline{\delta_m}} \tag{80}$$

If the Eqs. (80) and (79) are substituted in the Eq. (78), the following general expression is obtained, providing the 0.05 percentile of the debonding load:

$$\varepsilon_{th,k} = \varepsilon_{th,m} - 1.64 \cdot \varepsilon_{th,m} \cdot \left[a \cdot CoV_{E_f}{}^2 + b \cdot CoV_{f_{cm}}{}^2 + c \cdot CoV_{f_{ctm}}{}^2 + CoV_{\delta_m}{}^2\right]^{0.5} \tag{81}$$

where the coefficient a, b, c depend on the functional relationship of E_f, f_{cm} and f_{ctm} in the expression of ε_{th}; moreover the coefficients of variation are defined for each parameter as the ratio of the mean value to its standard deviation:

$$CoV_{E_f} = \frac{\overline{E_f}}{s_{E_f}},\ CoV_{f_{ctm}} = \frac{\overline{f_{ctm}}}{s_{f_{ctm}}},\ CoV_{f_{cm}} = \frac{\overline{f_{cm}}}{s_{f_{cm}}},\ CoV_{\delta_m} = \frac{\overline{\delta_m}}{s_{\delta_m}} \tag{82}$$

Clearly the coefficient of variation of the variable δ_m, $CoV_{\delta m}$, depends on the data distribution. The Eq. (81) can be written as:

$$\varepsilon_{th,k} = k_k \cdot \varepsilon_{th} \tag{83}$$

assuming:

$$k_k = k_m \cdot \left(1 - 1.64 \cdot \left[a \cdot CoV_{E_f}{}^2 + b \cdot CoV_{f_{cm}}{}^2 + c \cdot CoV_{f_{ctm}}{}^2 + CoV_{\delta_m}{}^2\right]^{0.5}\right). \tag{84}$$

Lower percentiles can be obtained by substituting in the Eq. (78) the coefficient 1.64, related to the 0.05 percentile of the frequency distribution, with the coefficients 2.58 and 3.08 corresponding to the 0.005 and 0.001 percentiles, respectively.

The use of percentiles lower than 0.05 can be alternative to the use of safety factors that usually have to be additionally applied to characteristic provision to take into account the model uncertainness (EN1990 – Annex D).
In Table 2 the coefficient k_m and the R^2, that is a measure of the reliability of the regression, are reported: two different experimental samples were considered for sheets and plates respectively. Note that for the cured-in-situ FRP systems (sheet) the R^2 value is quite high (0.855); on the contrary for the preformed systems (plate) the R^2 value is quite low (0.349), mainly due to a higher scattering of the experimental data.
In addition the mean value of the variable δ_m and its CoV are reported. In both cases the CoV, that represents a measure of the model significance, is lower than the threshold value of 40% (Monti et al., 2009) so that all the models can be considered reliable.
Finally, Table 2 shows that different scattering of experimental data leads to very different 0.05, 0.005 and 0.001 percentile of the calibrating coefficient k, for sheet and plate respectively.

FRP type	k_m	$\mathbf{R^2}$	$\overline{\delta_m}$	CoV_{δ_m}	$k_m \cdot \overline{\delta_m}$	$k_{k,5\%}$	$k_{k,0.5\%}$	$k_{k,0.1\%}$
Sheet	0.270	0.855	1.027	17.7%	0.278	0.192	0.143	0.117
Plate	0.236	0.349	1.064	23.2%	0.251	0.152	0.095	0.064

Table 2. Statistical data

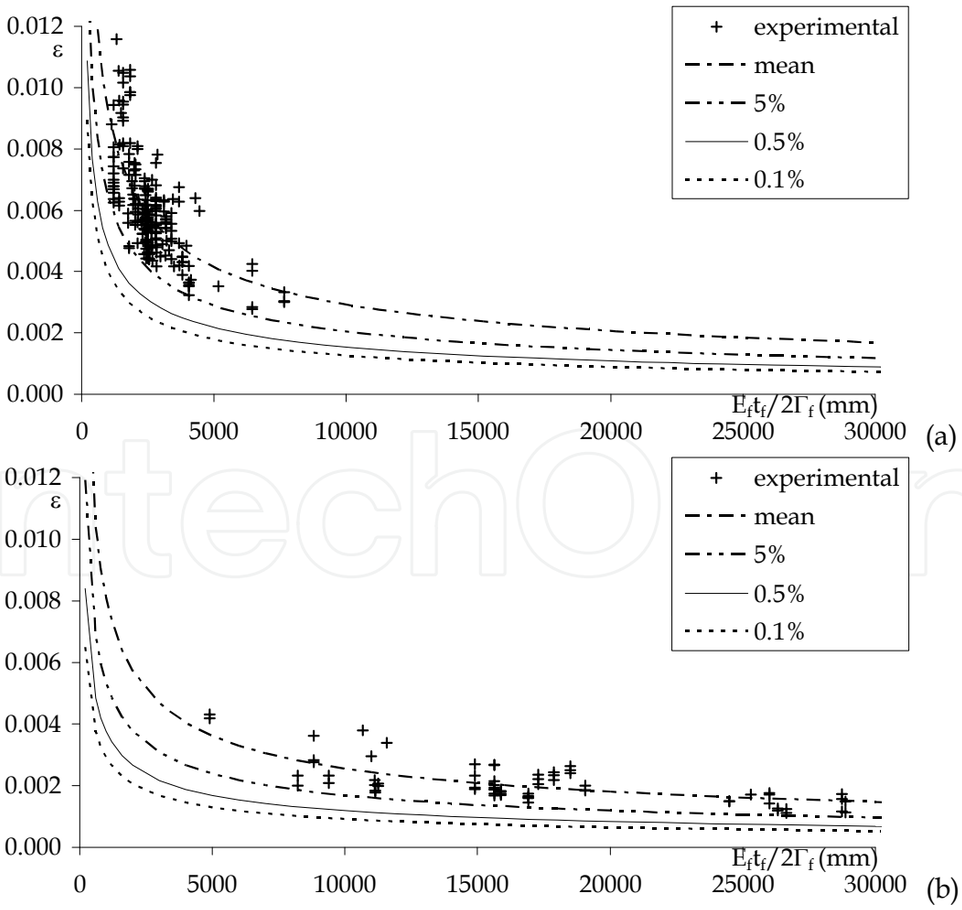

Fig. 17. Theoretical and experimental strains: sheets (a) and plates (b)

Theoretical debonding strain (71) are plotted in Fig. 17a,b versus the parameter $E_f t_f / k_b \sqrt{f_{cm} f_{ctm}}$, for sheets and plates respectively. Each curve is obtained with reference to each percentile of the k coefficient reported in Table 2. Theoretical debonding strains, obtained by means the calibrating procedure showed above, can be easily compared with experimental ones (singular point).

5. Conclusions

A wide overview of the key contributions in understanding the mechanical behavior of FRP laminates bonded on a concrete substrate has been reported in this chapter. Several original contributions have been also proposed.

First of all, a general analytical model has been formulated for describing the distribution of shear and normal stresses within the adhesive layer connecting the FRP laminate to the substrate. The key dimensionless parameters governing such distributions have been clearly pointed out and their influence has been showed in numerical application. The possible simplification of that general analytical model in a simpler one based on the assumption of a layer of elastic springs connecting the FRP laminate to the substrate has been also proposed.

This model leads to much simpler differential equations with a reasonable reduction of accuracy. Moreover, it can be easily extended to the nonlinear branch, especially in the case of a supposed bi-linear (namely, elastic-softening) behaviour of the interface in terms of relationship between shear stresses and interface slip. Closed-form solutions of the stress and strain distribution throughout the FRP laminate can be derived under this assumption.

Those closed-form solutions can be employed for identifying the actual properties of the interface relationship. The numerical stability of an indirect-identification procedure based on those solutions has been demonstrated in the section 3 of this chapter. Moreover, it has been showed that the experimental data can be simulated with good accuracy even if a simplified adhesion law (i.e. a bilinear adhesion law) is assumed.

The values of the mechanical properties of the adhesive FRP-to-concrete interface obtained by some experimental tests available in the scientific literature have been finally utilized for calibrating simplified design-oriented formulae for determining the values of the maximum axial strains which can be developed in the FRP laminate before the onset of the debonding phenomenon. The effect of both the material randomness and the model uncertainties in defining the characteristic value of the axial strain in FRP at debonding have been handled by means of a well-established statistical procedure.

6. References

Achintha P. M. M. & Burgoyne C. J. (2008). Fracture Mechanics of Plate Debonding, *ASCE Journal for Composites for Construction*, Vol. 12, No. 4, July/August 2009, 396-404, ISSN 1090-0268

ACI 440.2R-08 (2008). Guide for the Design and Construction of Externally Bonded FRP Systems for Strengthening Concrete Structures. *ACI440.2R-08* American Concrete Institute, Farmington Hills, MI, 2008, 76 pp.

Arduini M. & Nanni A. (1997). Behavior of precracked RC beams strengthened with carbon FRP sheets, *ASCE Journal for Composites for Construction*, Vol. 1, No. 2, 63–70, ISSN 1090-0268

Bilotta A., Ceroni F., Di Ludovico M., Nigro E. & Pecce M. (2011). Bond Tests on concrete elements strengthened with EBR and NSM FRP systems, *Proceedings of FRP RCS 10*, Tampa, Florida, April 2011, accepted.

Bilotta A., Ceroni F., Nigro E. & Pecce M. (2011). Design by testing of debonding load in RC element strengthened with EBR FRP materials, *Proceedings of FRP RCS 10*, Tampa, Florida, April 2011, accepted.

Bilotta A, Di Ludovico M. & Nigro E. (2009). Influence of effective bond length on FRP-concrete debonding under monotonic and cyclic actions. *Proceedings of 9th International Symposium on Fiber Reinforced Polymer Reinforcement for Concrete Structures,* Sydney (Australia), July 2009 (CD ROM).

Bizindavyi L. & Neale K. W. (1999). Transfer lengths and bond strengths for composites bonded to concrete, *ASCE Journal for Composites for Construction*, Vol. 3, No. 4, July/August 1999, 153-160, ISSN 1090-0268

Blontrock, H., Taerwe, L. & Vanwalleghem, H. (2002). Bond testing of externally glued FRP laminates at elevated temperature, *Proceedings of the International Symposium "Bond in Concrete: from research to standards"*, 648-654, ISBN 963-420-714-6, Budapest, November 2002, Publisher, City

Bonacci J.F. (1996). Strength, Failure Mode and Deformability of Concrete Beams Strengthened Externally with Advanced Composites, *Proceedings of the 2nd International Symposium on Advanced Composite Materials in Bridges and Structures*, ISBN, Montreal (Canada), 419-426, Publisher, City

Ceroni, F., Pecce, M., Matthys, S. & Taerwe, L. (2008). Bond tests on concrete elements with CFRP and anchorage systems, *Composites: Part B* - Elsevier, Vol. 39, No.3, April 2008, 429–441, ISSN 1359-8368

Ceroni F. & Pecce M. (2010). Evaluation of bond strength and anchorage systems in concrete elements strengthened with CFRP sheets, *ASCE Journal of Composites in Construction*, in press, ISSN 1090-0268

Chajes M.J., Finch W.W., Januszka T.F. & Thomson T.A. (1996). Bond and force transfer of composite-material plates adhered to concrete, *ACI Structural Journal*, Vol. 93, No. 2, February 1996, 208–217, ISSN 0889-3241

Chen J.F. & Teng J.G. (2001): Anchorage Strength Models for FRP and Plates Bonded to Concrete, *ASCE Journal of Structural Engineering*, Vol. 127, No. 7, July 2001, 784-791, ISSN 0733-9445

CNR-National Council for Research (2004), *Guide for the Design and Construction of Externally Bonded FRP Systems for Strengthening Existing Structures-Materials, RC and PC structures, masonry structures*

Czaderski C., Soudki K. & Motavalli M. (2010). Front and Side View Image Correlation Measurements on FRP to Concrete Pull-Off Bond Tests, *ASCE Journal for Composites for Construction*, Vol. 14, No. 4, July/August 2010, 451-463, ISSN 1090-0268

European Committee for Standardization. *EN 1990 – Eurocode - Basic of Structural Design*. 2002.

Faella C., Martinelli E. & Nigro E. (2002). Aderenza tra calcestruzzo e Lamine di FRP utilizzate come placcaggio di elementi inflessi. Parte II: modelli teorici ed

elaborazioni numeriche, Proceedings of the XIV C.T.E. Conference, Mantua (Italy), 7-8 November 2002, 237-245, (in Italian);

Faella C., Martinelli E. & Nigro E. (2008). Formulation and Validation of a Theoretical Model for Intermediate Debonding in FRP Strengthened RC Beams, *Composites Part B*, Vol. 39, No. 4, 645-655, June 2008, ISSN 1359-8368

Faella C., Martinelli E. & Nigro E. (2009). Direct versus Indirect Method for Identifying FRP-to-Concrete Interface Relationships, *ASCE Journal for Composites for Construction*, Vol. 13, No. 3, May/June 2009, 226-233, ISSN 1090-0268

fib Bulletin No. 14 (2001). *Externally bonded FRP reinforcement for RC structures*, Technical report, ISBN 978-2-88394-054-3, Lausanne (CH)

Hart-Smith, L. J. (1973). Adhesive-bonded double-lap joints, NASA Technical Report, CR-112235, Hampton, Va. (USA)

Lee Y. J., Boothby T. E., Bakis C. E. & Nanni A. (1999). Slip Modulus of FRP Sheets Bonded to Concrete, *ASCE Journal of Composites for Construction*, Vol. 3, No. 4, November 1999, 161-167, ISSN 1090-0268

Lu X.Z., Teng J.G., Ye L.P. & Jiang J.J. (2005). Bond-slip models for FRP sheets/plates bonded to concrete, *Engineering Structures*, Vol. 27, No. 6, May 2005, 920-937, ISSN 0141-0296

Mazzotti C., Savoia M. & Ferracuti B. (2009). A new single-shear set-up for stable debonding of FRP–concrete joints, *Construction and Building Materials - Elsevier*, Vol. 23, No.4, April 2009, pp. 1529-1537. ISSN 0950-0618

Malek A. M., Saadatmanesh H. & Ehsani M. R. (1998). Prediction of failure load of R/C beams strengthened with FRP plate due to stress concentration at the plate end, *ACI Structural Journal*, Vol. 95, No. 2, March/April 1998, 142-152, ISSN 1090-0268

Meier U. (1987). Brückensanierungen mit Hochleistungs-Faserverbundwerkstoffen, Material und Technik, Vol. 15, No 4, 125-128 ISSN

Meier U. (1995). Strengthening of structures using carbon fibre/epoxy composites, *Construction and Building Materials*, Vol. 9, No. 6, June 1995, 341–351, ISSN 0950-0618

Monti G., Alessandri S. & Santini S. (2009). Design by Testing: A Procedure for the Statistical Determination of Capacity Models, *Journal of Construction and Building Materials, Special Issue on FRP Composites Elsevier*, Vol. 23, 1487-1494. ISSN 0950-0618

Motavalli M. & Czaderski C. (2007). FRP Composites for Retrofitting of Existing Civil Structures in Europe: State-of-the-Art Review, *Proceedings of the American Composites Manufacturers Association 2007*, ISBN, Tampa, FL (USA), October 2007, Publisher, City

Naaman A.E., Park S.Y., Lopez M.M. & Till R.D. (2001). Parameters Influencing the Flexural Response of RC Beams Strengthened Using CFRP Sheets, *Proceedings of the Conference FRPRCS-5*, Cambridge (UK), 117-125, ISBN 0727730290

Neubauer, U. & Rostasy, F.S. (1997). Design Aspects of Concrete Structures Strengthened with Externally Bonded CFRP Plates, Concrete and Composites, *Procedings of 7th International Conference On Structural Faults and Repair*, Vol. 2, 109-118, ISBN, ECS Pub. Edinburgh, Scotland.

Nigro E., Di Ludovico M. & Bilotta A. (2008). FRP- Concrete Debonding: experimental Tests under Cyclic Actions, *Proceedings of 14th World Conference on Earthquake Engineering*, ISBN, Beijing (China), October 2008, Publisher, City

Oehlers D.J., Moran J.P. (1990). Premature failure of externally plated reinforced-concrete beams, *Journal of Structural Engineering - ASCE,* Vol. 116, No.4, April, 1990, 978-995. ISSN 0733-9445

Rabinovich O. & Frostig, Y. (2000). Closed-form High-order Analysis of RC Beams Strengthened with FRP Strips, *ASCE Journal of Composites for Construction*, Vol. 4, No. 2, March-April 2000, 65-74, ISSN 1090-0268

Rabinovich O. & Frostig, Y. (2001). Delamination Failure of RC Beams Strengthened with FRP Strips—A Closed-Form High-Oorder and Fracture Mechanics Approach, *Journal of Engineering Mechanics*, Vol. 127, No. 8, August 2001, ISSN 0733-9399

Roberts T.M. (1989). Approximate analysis of shear and normal stress concentrations in the adhesive layer of plated RC beams, *The Structural Engineer*, Vol. 67, No. 12, December 1989, 229–233, ISSN 0039-2553

Savoia M., Bilotta A., Ceroni F., Di Ludovico M., Fava G., Ferracuti B., Mazzotti C., Nigro E., Olivito R., Pecce M. & Poggi C., (2009). Experimental round robin test on FRP concrete bonding, *Proceedings of FRPRCS9*, Sydney (Australia), July, 2009 (CD ROM).

Smith S.T. & Teng J.G. (2001), Strength Models for Plate End Debonding in FRP-Strengthened RC Beams, *Proceedings of the Conference FRPRCS-5*, ISBN 0727730290, Cambridge (UK), 419-428, 2001, Publisher, City

Smith S. T. & Teng J. G. (2002). FRP-strengthened RC beams. I: review of debonding strength models, *Engineering Structures*, Vol. 24, No. 4, April 2002, 385-395, ISSN 0141-0296

Swamy R.N., Jones R. & Bloxham J.W. (1987). Structural behaviour of reinforced concrete beams strengthened by epoxy-bonded steel plates, *The Structural Engineer*, Vol. 65A, No. 2 February 1987, 59–68, ISSN 0039-2553

Taljsten B. (1996). Strengthening of concrete prisms using the plate bonding technique, *International Journal of Fracture*, Vol. 82, No., 253–266, ISSN 0376-9429

Taljsten B. (1997). Strengthening of beams by plate bonding, *ASCE Journal of Materials in Civil Engineering*, Vol. 9, No. 4, November 1997, 206–211, ISSN 1943-5533

Teng J.G., Chen J.F., Smith S.T. & Lam L. (2002). *FRP Strengthened RC Structures*, John Wiley & Sons Ltd., ISBN 0-471-48706-6, 245pp. Chichester (UK)

Teng J. G., Smith S. T., Yao J. & Chen J. F. (2003). Intermediate crack-induced debonding in RC beams and slabs, *Construction and Building Materials*, Vol. 17, No. 6-7, September-October 2003, 447-462, ISSN 0950-0618

Tounsi A., Hassaine Daouadji T., Benyoucef S. & Addabedia E.A. (2009). Interfacial stresses in FRP-plated RC beams: Effect of adherend shear deformations, *International Journal of Adhesion & Adhesives – Elsevier,* Vol. 29, No. 4, June, 2009, 343-351, ISSN 0143-7496

Triantafillou T., Matthys S. & Taerwe L. (2001). Design of Concrete Members Strengthened with Externally Bonded FRP Reinforcement, *Proceedings of the Conference FRPRCS-5*, Cambridge (UK), 157-166, ISBN 0727730290, Publisher, City

Wu, Z., Yuan, H. & Niu, H. (2002). Stress transfer and fracture propagation in different kinds of adhesive joints, *ASCE Journal of Engineering Mechanics*, Vol. 128, No. 5, May 2002, 562-573, ISSN: 0733-9399

Yao J., Teng J.G. & Chen J.F. (2005). Experimental study on FRP-to-concrete bonded joints, *Composites: Part B*, Elsevier, Vol. 36, No. 2, March, 2005, 99–113, ISSN 1359-8368

Yuan H., Chen J.F., Teng J.G., Lu X.Z. (2007). Interfacial stress analysis of a thin plate bonded to a rigid substrate and subjected to inclined loading, *International Journal of Solids and Structures*, Vol. 44, No. 16, August 2007, ISSN 0020-7683

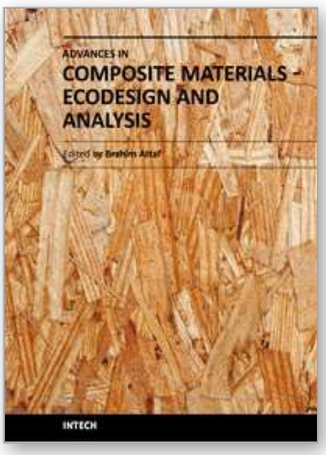

Advances in Composite Materials - Ecodesign and Analysis
Edited by Dr. Brahim Attaf

ISBN 978-953-307-150-3
Hard cover, 642 pages
Publisher InTech
Published online 16, March, 2011
Published in print edition March, 2011

By adopting the principles of sustainable design and cleaner production, this important book opens a new challenge in the world of composite materials and explores the achieved advancements of specialists in their respective areas of research and innovation. Contributions coming from both spaces of academia and industry were so diversified that the 28 chapters composing the book have been grouped into the following main parts: sustainable materials and ecodesign aspects, composite materials and curing processes, modelling and testing, strength of adhesive joints, characterization and thermal behaviour, all of which provides an invaluable overview of this fascinating subject area. Results achieved from theoretical, numerical and experimental investigations can help designers, manufacturers and suppliers involved with high-tech composite materials to boost competitiveness and innovation productivity.

InTech Europe
University Campus STeP Ri
Slavka Krautzeka 83/A
51000 Rijeka, Croatia
Phone: +385 (51) 770 447
Fax: +385 (51) 686 166
www.intechopen.com

InTech China
Unit 405, Office Block, Hotel Equatorial Shanghai
No.65, Yan An Road (West), Shanghai, 200040, China
中国上海市延安西路65号上海国际贵都大饭店办公楼405单元
Phone: +86-21-62489820
Fax: +86-21-62489821

IntechOpen